When Large Vision-Language Model Meets Large Remote Sensing Imagery: Coarse-to-Fine Text-Guided Token Pruning

Junwei Luo[1*], **Yingying Zhang**[2], **Xue Yang**[3], **Kang Wu**[1*], **Qi Zhu**[4*],
Lei Liang[2], **Jingdong Chen**[2], **Yansheng Li**[1‡]
[1]Wuhan Universtiy   [2]Ant Group
[3]Shanghai Jiao Tong University   [4]University of Science and Technology of China
{luojunwei,kangwu,yansheng.li}@whu.edu.cn
{qichu.zyy,leywar.liang,jingdongchen.cjd}@antgroup.com
yangxue-2019-sjtu@sjtu.edu.cn   zqcrafts@mail.ustc.edu.cn
https://github.com/VisionXLab/LRS-VQA

Abstract

Efficient vision-language understanding of large Remote Sensing Images (RSIs) is meaningful but challenging. Current Large Vision-Language Models (LVLMs) typically employ limited pre-defined grids to process images, leading to information loss when handling gigapixel RSIs. Conversely, using unlimited grids significantly increases computational costs. To preserve image details while reducing computational complexity, we propose a text-guided token pruning method with Dynamic Image Pyramid (DIP) integration. Our method introduces: (i) a Region Focus Module (RFM) that leverages text-aware region localization capability to identify critical vision tokens, and (ii) a coarse-to-fine image tile selection and vision token pruning strategy based on DIP, which is guided by RFM outputs and avoids directly processing the entire large imagery. Additionally, existing benchmarks for evaluating LVLMs' perception ability on large RSI suffer from limited question diversity and constrained image sizes. We construct a new benchmark named LRS-VQA, which contains 7,333 QA pairs across 8 categories, with image length up to 27,328 pixels. Our method outperforms existing high-resolution strategies on four datasets using the same data. Moreover, compared to existing token reduction methods, our approach demonstrates higher efficiency under high-resolution settings.

1. Introduction

Benefiting from the rapid advancement of Large Language Models (LLMs) [1, 9, 12, 15, 67], Large Visual-Language Models (LVLMs) have demonstrated strong capabilities in
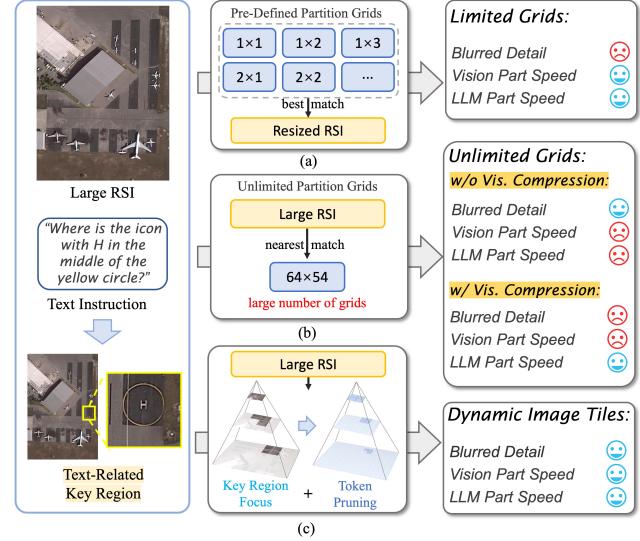

Figure 1. High-resolution strategy comparison for modular LVLMs. (a) and (b) show existing grid-based cropping methods face challenges when processing large RSIs. (c) The proposed dynamic pyramid-based token pruning strategy can dynamically select image tiles of key regions related to the input text, balancing image detail and computational cost.

perceiving and understanding visual information in text-based multimodal interactions [7, 25, 35, 57]. Currently, LVLMs have been extensively studied and applied across various fields like remote sensing (RS) intelligent interpretation [10, 28, 43, 46, 65, 75, 79].

Advances in satellite imaging technology allow for the acquisition of large remote sensing images (RSIs) that cover extensive ground areas and contain detailed land use information. Therefore, natural language-based intelligent analysis of large RSIs is valuable for applications such as com-

---

plex scene understanding [33], urban planning [31, 56], infrastructure development [62], and monitoring [85].

Some RS LVLMs handle high-resolution input through position embedding interpolation [24, 78]. Additionally, various dynamic high-resolution strategies designed for general LVLMs [29, 35, 72] can be adapted to RS LVLMs, such as EarthDial [53] (based on InternVL1.5 [8]) and GeoPixel [49] (using InternLM-XComposer2.5 [76]). However, these approaches for high-resolution image processing are limited when handling large RSIs exceeding 10,000×10,000 pixels. As depicted in Fig. 1, these methods typically employ limited pre-defined grid partitions, leading to detail loss when large RSIs are excessively downsampled. Conversely, unlimited grids suffer from prohibitive time and memory costs (e.g., over 5 million vision tokens for a large RSI in LLaVA-1.5 [35]). This necessitates balancing resolution and computational efficiency when processing large RSI.

To overcome the above limitations of existing strategies in handling large RSIs, we propose a text-guided token pruning strategy that consists of two key components: a Region Focus Module (RFM) and a Dynamic Image Pyramid (DIP). The RFM identifies text-relevant key vision tokens by leveraging the capability distilled from the LLM component. Based on the RFM's output, we select critical image tiles and conduct token pruning in a coarse-to-fine manner within the DIP. This enables the LVLM to focus and zoom in key areas, avoiding to process all visual tokens, thereby facilitating flexible and efficient inference.

Moreover, benchmarks for LVLMs in understanding large RSIs remain insufficiently developed. Although MME-Realworld [83] includes large RSIs with high-quality manually annotated questions, its RS subset suffers from limited question diversity and image sizes. To more comprehensively characterize the challenges of large RSI perception, we construct a new benchmark called LRS-VQA (**L**arge **R**emote **S**ensing image Visual Question Answering). LRS-VQA features larger size images with lengths up to 27,328 pixels and 8 distinct question types. Our key contributions are as follows:

- We introduce a Region Focus Module (RFM) that distills the ability from LLM part of LVLM to efficiently identify text-related key vision tokens.
- Based on RFM and DIP, we propose an efficient coarse-to-fine inference strategy for large RSIs, which achieves a balance between resolution and efficiency through key tile selection and vision token pruning.
- We construct a new benchmark named LRS-VQA, featuring larger image sizes and more diverse question types than existing benchmarks, to reflect the challenges of large RSIs perception.
- The proposed method is architecture-agnostic and shows performance improvements and efficiency gains.

2. Related Work

2.1. LVLMs for High-Resolution Comprehension

Numerous LVLMs designed for high-resolution image or video perception have recently emerged. They can be primarily categorized into the following paradigms:

Methods that carefully design image cropping and padding strategy. Methods like [8, 16, 25, 34, 35, 38, 72, 82] traverse pre-defined partition grids and obtain the most suitable grid, to divide the high-resolution image into image tiles. These methods encounter limitations when processing large RSIs as in Fig. 1.

Methods based on multiple visual branches. These approach [30, 42, 55] employ additional high-resolution visual encoders like SAM [22] encoder or ConvNext [39] to process images with higher input resolution.

Visual chain-of-thoughts methods. These approaches utilize a search-and-focus strategy [51, 52, 58, 61] or external RAG pipeline [84] to identify text-related key image regions. However, such pipelines require multiple LVLM inferences, making them more complex and cumbersome.

2.2. Vision Token Reduction in LVLMs

Visual token pruning for transformers has been a classic research topic, it aims to accelerate computation by dynamically reducing less important tokens. It has been extensively studied in both natural language processing [21, 71] and computer vision domains [14, 23, 44, 48, 60].

Recently, a variety of token pruning methods have been proposed for LVLMs, which can be categorized into three main types: token pruning conducted in the vision encoder [4, 29, 50, 59, 69, 70], token pruning performed in the LLM component [6, 17, 18, 64, 73, 80], and collaborative approaches that integrate both [5, 26, 27, 32, 66, 74, 77].

Although vision-part pruning methods efficiently reduce vision tokens, when processing large images, it's highly time-consuming to traverse pre-defined grids and handle numerous image tiles with the vision encoder. Moreover, the absence of language guidance makes it hard to identify foreground regions in complex RSIs. The LLM-part pruning methods require feeding all vision tokens into the LLM. Therefore, long visual sequences from large images may exceed LLM length limits and incur high computational costs for attention score ranking.

Among the collaborative approaches, the methods most closely related to ours are LLaVA-Mini [77] and FlexAttention [27]. The former employs modality pre-fusion to compress visual information; however, its LLM-like pre-fusion module still struggles with handling extremely long vision sequences. The latter integrates text-guided high-resolution features within the LLM component. Nevertheless, the allowable image size for its high-resolution view remains limited, and it can only index high-resolution features once.
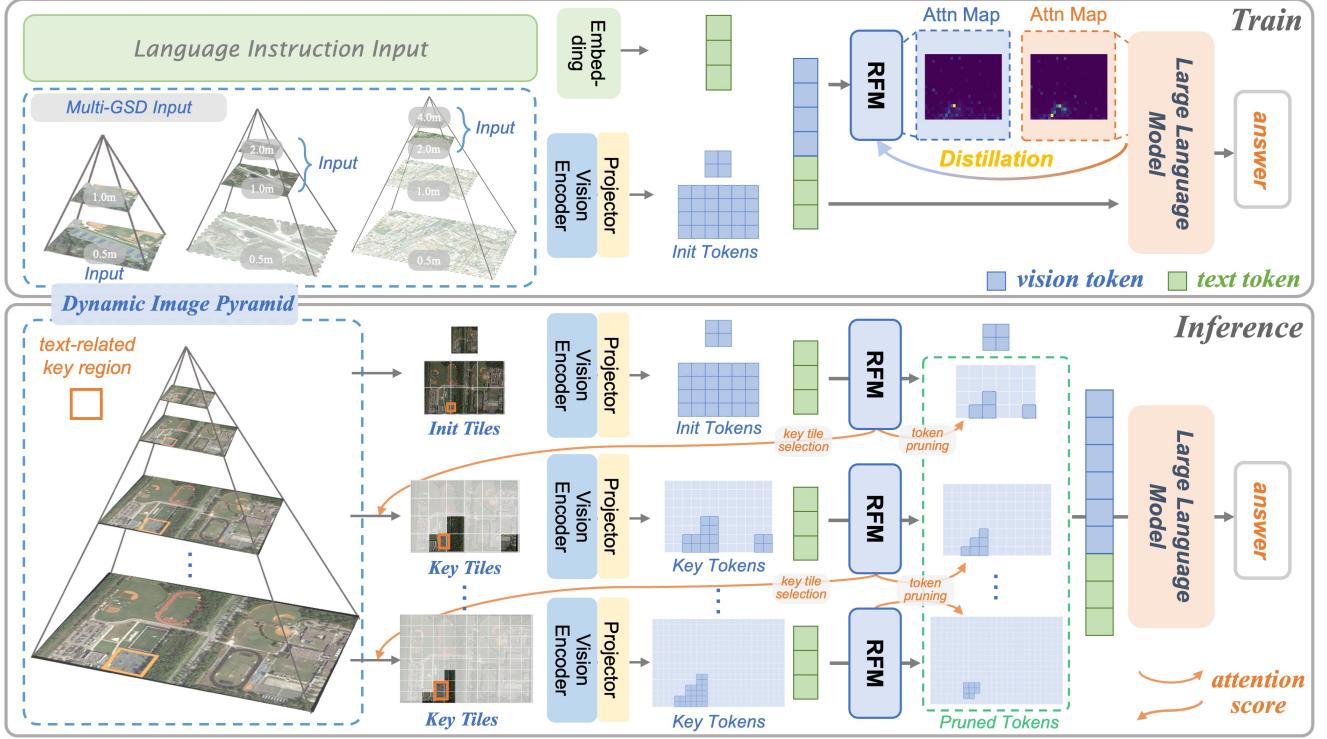
Figure 2. The pipeline of the proposed method. The entire process iterates in a coarse-to-fine manner, dynamically retrieving high-resolution features from the next DIP level (leftward orange arrow) or performing token pruning at the current level (rightward orange arrow) based on the output of the RFM module at each iteration. During training, the RFM distillation text-related attention from the LLM; during inference, RFM generates the attention scores for the input vision tokens. GSD means ground sample distance.

3. Preliminaries

In this section, we present the foundational concepts of text-image attention within the LLM component of high-resolution LVLMs. The proposed RFM leverages this mechanism to guide the text-related key image tile selection and the vision token pruning.

Mainstream modular LVLMs include three components [41]: a pre-trained vision encoder, a feature projector, and a pre-trained decoder-only LLM. Conventional high-resolution strategies [8, 16] process the original image I_{img} into a thumbnail view I_{thumb} and a set of image tiles I_{tiles}. Then the vision encoder and the projector transforms I_{thumb} and I_{tiles} into vision token embeddings $T_{vis} = [T_{vis}^{lr}, T_{vis}^{hr}]$, which contain low-resolution tokens T_{vis}^{lr} from the I_{thumb} and higher-resolution T_{vis}^{hr} from the I_{tiles}. T_{vis} are concatenated with text token embeddings T_{txt} from the tokenized text instruction, forming a multimodal token sequence $T = [T_{vis}, T_{txt}]$. The LVLM processes T via transformer-based decoder layers with causal self-attention, where the attention score A can be represented as:

$$A = \text{Attention}(Q, K) = \text{Softmax}\left(\frac{QK^\top}{\sqrt{d}}\right), \quad (1)$$

where $A \in \mathbb{R}^{n \times n}$ is the self-attention map, $Q, K \in \mathbb{R}^{n \times d}$ are the query and key matrices derived from the input embeddings through linear transformations, n is the input sequence length, and d is the feature dimension. As A determines the weight each token assigns to the former tokens in the sequence, by analyzing the attention from text tokens to vision tokens, we can identify text-related important vision tokens. Some studies [20, 73] observe that in the deep layers of LLM part in LVLMs, attention is predominantly allocated to text-related vision tokens compared to other vision tokens. This insight inspired us to design a coarse-to-fine mechanism to focus on key image regions.

4. Method and Benchmark

4.1. Method

To achieve efficient high-resolution image understanding, we propose a method that combines text-guided key region localization with a multi-level dynamic image pyramid (DIP), as shown in Fig. 2. Initially, the DIP is constructed based on the input large image. At the low-resolution DIP level, the Region Focus Module (RFM) provides attention distribution for the initial vision tokens. These result guides the retrieval of corresponding image tiles from
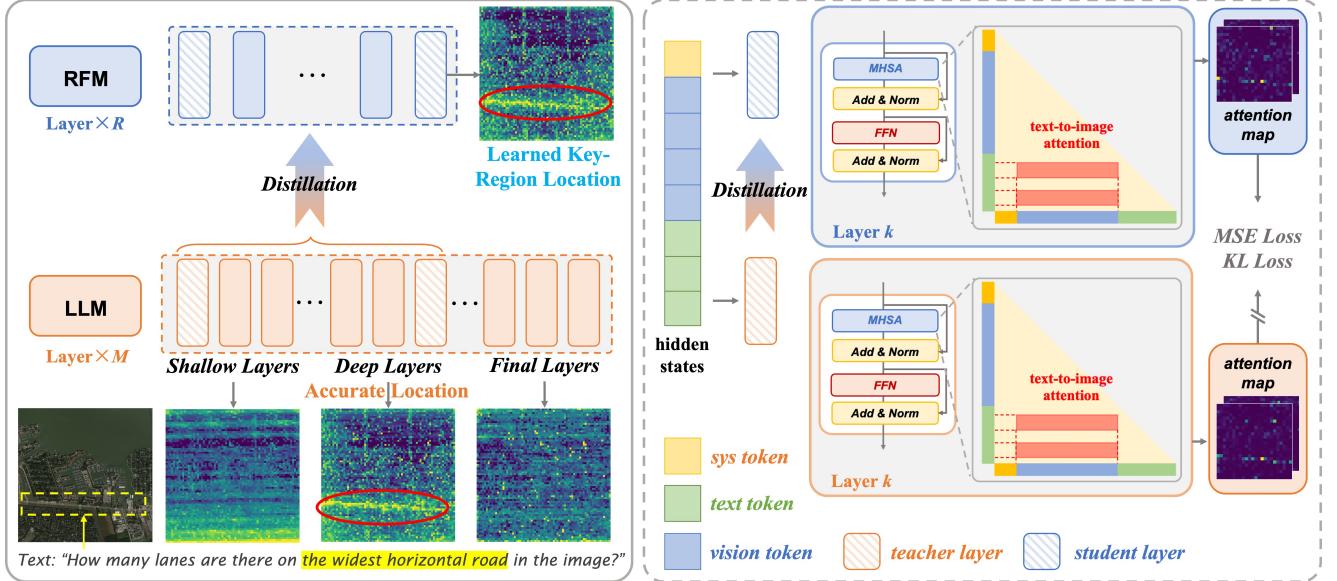
3

Figure 3. The proposed RFM and attention distillation strategy. The left part indicates our core idea: distill accurate text-related key region localization ability from the LLM part of the LVLM. The right part shows the distillation details. We only select specific layer pairs for distillation to avoid hidden state discontinuities. "sys token" represents the tokens from the system prompt.

higher-resolution DIP levels or trigger token pruning at the current level. This iterative process could continue through the pyramid until reaching the original resolution. Below, we introduce our approach in three components: DIP construction in Sec. 4.1.1, RFM and attention distillation in Sec. 4.1.2, and their integration in Sec. 4.1.3.

4.1.1. The Construction of Dynamic Image Pyramid

Given an original large RSI I_{img}, we construct an image-level pyramid with a variable number of layers to generate a series of image tiles at different ground sample distances (GSDs), enabling coarse-to-fine inference.

First, we iteratively downsampling I_{img} by a factor of 2, generating a series of images $\{I_{init}^1, I_{init}^2, \ldots, I_{init}^P\}$ until the shorter side reaches a pre-defined minimum length. Let a basic image tile size be $B \times B$ (e.g., 336×336 for CLIP-L14), for the p-th scaled image I_{init}^p, we calculate the number of image tiles along the height and width as follows:

$$N_h^p = \lceil H_p/B \rceil, \quad N_w^p = \lceil W_p/B \rceil, \quad (2)$$

where H_p, W_p are the height and width of I_{init}^p, respectively. For proper tiling, we compute a scale factor r_p as:

$$r_p = \min\left(\frac{N_h^p \times B}{H_p}, \frac{N_w^p \times B}{W_p}\right). \quad (3)$$

The image I_{init}^p is then resized to I^p using r_p, followed by padding to preserve the original aspect ratio. After resizing, I^p is partitioned into non-overlap tiles I_{tiles}^p. Tiles from all scaled images are combined in reverse order, and integrated with the thumbnail view I_{thumb} to form the final

pyramid: $I_{DIP} = \{I_{thumb}, I_{tiles}^1, I_{tiles}^2, \ldots, I_{tiles}^P\}$, which consists of $P + 1$ layers with progressively increasing resolutions. During training, we select the thumbnail I_{thumb} and I_{tiles}^1 as visual inputs for computational efficiency. During inference, all pyramid layers become accessible to enable multi-scale inference, as in the left part of Fig. 2.

4.1.2. Attention Distillation for Key Region Focus

In this section, we introduce the core idea and details of the Region Focus Module (RFM), a lightweight module designed to replicate the text-guided region localization capability inherent in LVLM's LLM part. RFM can be seamlessly integrated during the supervised fine-tuning (SFT) stage of LVLM, and generates attention scores for vision tokens during inference.

Prior findings [20, 64, 73] demonstrate that the deep layers in the LLM part of LVLM could accurately localize text-related key regions in the image through cross-model attention. Inspired by this observation, our core idea is to distill this text-guided key region focus capability from the LLM, as shown in the left part of Fig. 3. After distillation, the trained RFM can help to select text-related key image tiles and prune vision tokens before the LLM, reducing computational overhead from the image encoding stage.

Specifically, assuming the LLM has M layers $l_1, l_2, \ldots, l_M$, the proposed RFM adopts the same architecture with R layers $r_1, r_2, \ldots, r_R$, where $R<M$. Each RFM layer r_i is initialized from a selected LLM layer l_{m_i}, where $\{m_1, m_2, \ldots, m_R\}$ forms a sparse subset of LLM layer indices. For layer-wise distillation, we select K pairs ($K<R$) from RFM and LLM as student-teacher pairs,

represented as $\{(r_k, l_{m_k}) \mid k = 1, 2, \ldots, K\}$. This strategy avoids rigidly aligning each r_i with l_{m_i}, which would neglect the non-teacher layers in the LLM, resulting in inconsistency between adjacent RFM layers when training.

As depicted in the right part of Fig. 3, the concatenated multimodal tokens $T = [T_{vis}, T_{txt}]$ are fed into both the RFM and the LLM during training. For the k-th student-teacher layer pair (r_k, l_{m_k}), we extract the attention scores between the last text token and all vision tokens from the multi-head self attention (MHSA). For the h-th head, the self-attention is represented as $A_{\text{stu}}^{k,h}, A_{\text{tea}}^{k,h} \in \mathbb{R}^{j \times n_v}$, where j is the number of dialogue turns for multi-turn instruction and n_v is the length of vision tokens. We apply the Kullback-Leibler (KL) divergence loss for distillation:

$$\mathcal{L}_{\text{kl}}^h = \sum_{k=1}^K \left[D_{\text{KL}} \left(A_{\text{tea}}^{k,h} \parallel A_{\text{stu}}^{k,h} \right) + \lambda_{\text{hr}} D_{\text{KL}} \left(A_{\text{tea}}^{k,h,\text{hr}} \parallel A_{\text{stu}}^{k,h,\text{hr}} \right) \right], \tag{4}$$

where $A_{\text{tea}}^{k,h,\text{hr}}, A_{\text{stu}}^{k,h,\text{hr}}$ denote attention corresponding to T_{vis}^{hr}, and λ_{hr} is the weighting factor. Additionally, we enforce stronger alignment constraints to the attention of T_{vis}^{hr} by using an additional Mean Squared Error (MSE) loss:

$$\mathcal{L}_{\text{mse}}^h = \sum_{k=1}^K \text{MSE} \left(A_{\text{stu}}^{k,h,\text{hr}}, A_{\text{tea}}^{k,h,\text{hr}} \right). \tag{5}$$

The total distillation loss is computed as:

$$\mathcal{L}_{\text{distill}} = \frac{1}{KH} \sum_{h=1}^H \left(\lambda_{\text{mse}} \mathcal{L}_{\text{mse}}^h + \lambda_{\text{kl}} \mathcal{L}_{\text{kl}}^h \right), \tag{6}$$

where K is the number of selected student-teacher layer pairs, H is the number of attention heads, and $\lambda_{\text{mse}}, \lambda_{\text{kl}}$ are hyperparameters. For the flash-attention [11], we employ a specialized value matrix to extract attention maps like [80] to ensure compatibility.

4.1.3. Text-Guided Token Pruning with Pyramid

Given the extensive irrelevant background content in large RSIs, the core of our strategy lies in iteratively selecting text-related key image tiles and performing token pruning, thereby achieving a coarse-to-fine inference, as illustrated in the below part of Fig. 2.

Specifically, we integrate DIP and RFM for inference, as detailed in Alg. 1. For simplicity, the tokens from the system prompt are omitted. We initialize the vision input using I_{thumb} and I_{tiles}^p to generate the initial $T_{vis} = [T_{vis}^{lr}, T_{vis}^{p,hr}]$, where $p = 1$, then the concatenated tokens T are fed into the RFM. From the last layer of the RFM, we compute the average attention scores from all heads in the MHSA, and extract the attention scores $A_{\text{stu}}^{K,hr}$ of $T_{vis}^{p,hr}$. By selecting the top-λ proportion from $A_{\text{stu}}^{K,hr}$, we identify the indices of key tokens and map their coordinates to image tile-level coordinates, to select key image tiles I_{key}^{p+1} from I_{tiles}^{p+1}. Based

---

Algorithm 1 Coarse-to-Fine Token Pruning with DIP

Require: $\{I_{\text{tiles}}^1, I_{\text{tiles}}^2, \ldots, I_{\text{tiles}}^P\}$ in I_{DIP}, K-layer RFM, initial multimodal tokens T, vision encoder and projector $\mathcal{V}(\cdot)$, token saving ratio α, tile number threshold $N_{\max}$

Ensure: Retained tokens $T_{\text{vis}}^{\text{retain}}$

1: **Definition:** Top-$\alpha(X)$ selects elements in X with values in the top α proportion.
2: **for** $p = 1$ **to** P **do**
3:     Compute attention: $A_{\text{stu}}^{K,hr} \leftarrow \text{RFM}(T)[T_{\text{vis}}^{p,hr}]$
4:     Normalize:
5:     Identify key positions: $\mathcal{P}_{\text{key}}^{K,hr} \leftarrow \text{Top-}\alpha(A_{\text{stu}}^{K,hr})$
6:     **if** $p < P$ **then**
7:         Map coordinates and select key tiles: $I_{\text{key}}^{p+1} \leftarrow \{t \in I_{\text{tiles}}^{p+1} \mid \text{mapped from } \mathcal{P}_{\text{key}}^{K,hr}\}$
8:         **if** $|I_{\text{key}}^{p+1}| > N_{\max}$ **then**
9:             Prune tokens: $T_{\text{vis}}^{\text{retain}} \leftarrow \{t \in T_{\text{vis}}^{p,hr} \mid \mathcal{P}_{\text{key}}^{K,hr}\}$
10:             **break**
11:         **else**
12:             Encode selected tiles: $T_{\text{vis}}^{p+1,hr} \leftarrow \mathcal{V}(I_{\text{key}}^{p+1})$
13:             Update $T \leftarrow [T_{\text{vis}}^{lr}, T_{\text{vis}}^{p+1,hr}, T_{\text{txt}}]$
14:         **end if**
15:     **else**
16:         Prune tokens at final layer: $T_{\text{vis}}^{\text{retain}} \leftarrow \{t \in T_{\text{vis}}^{p,hr} \mid \mathcal{P}_{\text{key}}^{K,hr}\}$
17:     **end if**
18: **end for**
19: **return** $T_{\text{vis}}^{\text{retain}}$

---

on the number of I_{key}^{p+1}, we determine whether to prune the $T_{\text{vis}}^{p,hr}$ directly or replace it with vision tokens $T_{\text{vis}}^{p+1,hr}$ from higher-resolution tiles. If $T_{\text{vis}}^{p+1,hr}$ is obtained, the tile selection process is repeated recursively until the last layer of DIP is reached. This approach enables LVLM to focus only on processing a few high-resolution image tiles in a coarse-to-fine manner, thereby reducing computational complexity while preserving critical text-related image details.

4.2. The Construction of LRS-VQA Benchmark

Considering the limitations of existing benchmarks for evaluating LVLMs' perception of RSIs in terms of question diversity and image size, we propose a new benchmark for more comprehensively evaluation.

4.2.1. Annotation Pipeline

The annotation pipeline of LRS-VQA is illustrated in Fig. 4. We collect 3 publicly remote sensing datasets: FAIR1M-1.0 [54], GLH-Bridge [31], and STAR [33], and identify all unique targets based on the object detection labels to generate unique references from them (e.g., "the top-most ship" and "the largest dock"). Subsequently, we crop the region with the unique target from the original image, and feed it, along with a prompt containing the unique reference, into

Dataset	Image Size	Image Num	Ques. Cate.	Ques. Num	QS Format
MME-RealWorld-RS [83]	689-11500	1298	3	3738	Single-choice
LRS-VQA (Ours)	1024-27328	**1657**	**8**	**7333**	Open-end

Table 1. Comparison of existing benchmarks for evaluating LVLMs' perception capabilities in large RSIs.
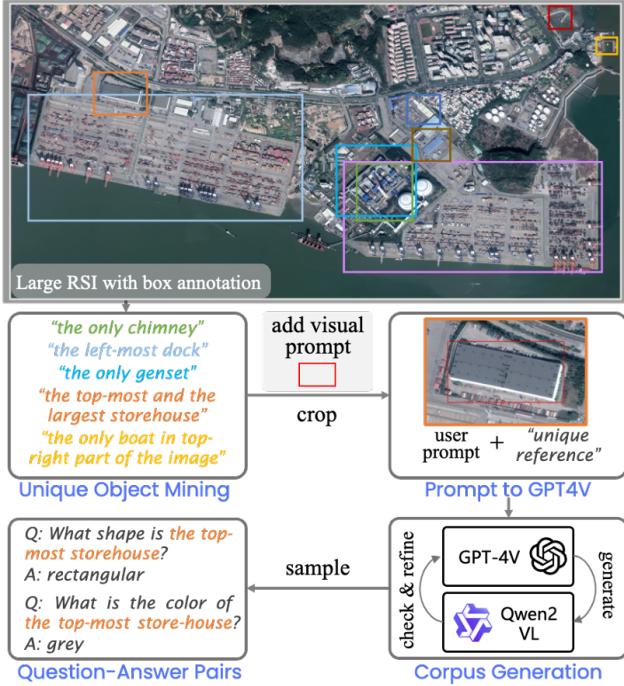

Figure 4. The construction pipeline of the proposed LRS-VQA dataset. The visual prompt (red box) is inspired by SoM [68].

GPT-4V [47] to generate question-answer pairs about the target's color, shape, status, etc. Details of the overall construction process are provided in the Appendix A.1.

4.2.2. Visual-Centric Quality Check and Refinement

To ensure the quality of the generated question-answer pairs, we employ powerful Qwen2-VL [57] for quality assessment. Qwen2-VL supports manual adjustment of the maximum pixel resolution, allowing us to evaluate whether increased resolution improves accuracy while keeping the LLM unchanged. Using this approach, we filter out question types where accuracy can not improve with resolution. Through iterative filtering, manual review, and prompt refinement, we obtain the LRS-VQA dataset, which could effectively assess the large RSI perception capability of LVLMs, as shown in Fig. 5. LRS-VQA contains eight question-answer types: *count, color, category, shape, status, reasoning, rural/urban classification, and target background*. It features greater diversity in question types and larger image sizes than MME-Realworld-RS as in Tab. 1, highlighting the complexities of large RSI perception.
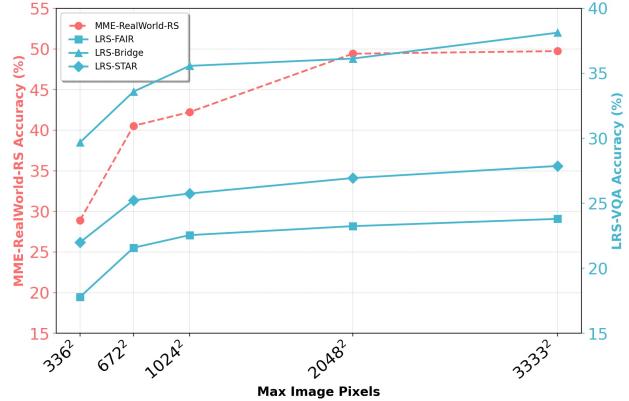

Figure 5. The accuracy trends of Qwen2-VL across varying input maximum pixels. This demonstrates that accuracy on both the manually annotated MME-RealWorld-RS and our proposed LRS-VQA exhibit a positive correlation with resolution improvement, proving the effectiveness of LRS-VQA in evaluating LVLM's high-resolution RSI perception capabilities.

5. Experiments

5.1. Experimental Details

Data. During the pre-training (PT) phase, we utilized the same 558K data used in LLaVA-1.5 [36]. For the SFT phase, we collect 484K samples, including 300K sampled from LLaVA-1.5-665K, 146K sampled from RSVQA-HR [40], and 38K template-based samples from 3 RS datasets [13, 31, 33] using their labels. Note some images in this 38k data are from the same source as LRS-VQA, but there is no overlap or duplication between them. Details can be found in the Appendix A.2.1.

Benchmarks and evaluation metrics: i) MME-RealWorld-RS: the RS part of MME-Realworld [83], containing 1,298 RSIs with expert-annotated questions in three types: color, count, and position. We follow the official evaluation script but modify the prompt by removing "The best answer is:" to address Vicuna-1.5-based models' tendency to respond with only option A. ii) LRS-VQA: it consists of 3 parts: LRS-FAIR, LRS-Bridge, and LRS-STAR, containing 2,272, 1,062, and 3,999 QA pairs, respectively. For the short open-ended format, we adopt a structured evaluation metric following [19, 63], using WordNet [45], with a semantic similarity threshold of 0.8.

Experimental settings. We employ existing LVLMs' official weights or api for evaluation. For comparison,

6

Leaderboard	Data	Vis. Encoder	LLM	Max Size	MME-RW-RS	LRS-FAIR	LRS-Bridge	LRS-STAR	Avg. Acc
Qwen2-VL [57]	-	QwenViT	Qwen2-7B	3,333×3,333	49.73	23.80	38.12	27.87	34.88
LLaVA-OV [25]	4.8M	SigLip	Qwen2-7B	2,304×2,304	53.53	20.61	35.11	26.08	33.83
IXC-2.5 [76]	-	CLIP-L14	InternLM2-7B	4,096×4,096	36.12	25.25	38.41	27.30	31.77
LLaVA-UHD-v2 [81]	1.42M	CLIP-L14+JBU	Vicuna-1.5-7B	672×1,008	40.77	22.82	32.57	26.08	30.56
LLaVA-FlexAttn [27]	1.22M	CLIP-L14	Vicuna-1.5-7B	1,008×1,008	37.75	19.57	29.99	22.76	27.52
SEAL [61]	0.95M	CLIP-L14	Vicuna-1.5-7B	-	30.55	21.29	34.75	21.29	26.97
MGM-HD [30]	3.0M	Mixed	Vicuna-1.5-7B	1,536×1,536	31.51	17.90	35.92	20.13	26.36
SLiME [82]	2.0M	CLIP-L14	Vicuna-1.5-7B	672×1,008	28.54	17.11	32.09	22.99	25.18
LLaVA-1.5 [35]	1.22M	CLIP-L14	Vicuna-1.5-7B	336×336	26.38	18.76	30.70	22.63	24.62
RSUniVLM [37]	1.2M	SigLip	Qwen2-0.5B	336×336	25.39	21.02	32.61	24.72	25.93
Geochat [24]	1.53M	CLIP-L14	Vicuna-1.5-7B	504×504	28.62	20.18	24.54	13.75	21.77
GPT-4o [2]	-	-	-	-	28.92	22.15	31.84	27.40	27.58
GPT-4o-mini [2]	-	-	-	-	6.69	18.67	31.99	25.85	20.80
Claude-3.5-Sonnet [3]	-	-	-	-	25.74	12.95	26.69	13.29	19.67
Comparison									
LLaVA-1.5*		CLIP-L14		336×336	34.40	18.24	32.28	24.17	27.30
LLaVA-1.5-p4*		CLIP-L14		672×672	38.20	19.18	35.43	_26.50_	29.83
Geochat*	1.04M	CLIP-L14	Vicuna-1.5-7B	504×504	33.68	21.51	35.97	25.86	29.25
SLiME*		CLIP-L14		672×1,008	34.56	_21.98_	33.20	25.10	28.71
LLaVA-UHD-v2*		CLIP-L14+JBU		672×1,008	_38.55_	20.77	_36.57_	25.79	_30.42_
Ours (LLaVA-1.5)		CLIP-L14		Dynamic	**39.04**	**22.97**	**36.89**	**27.48**	**31.59**
LLaVA-Next-p4*				672×672	39.12	21.06	36.27	25.80	30.56
LLaVA-Next-p9*	1.04M	CLIP-L14	Qwen2-7B	1,008×1,008	_40.35_	_21.14_	_37.25_	26.10	_31.21_
LLaVA-Next-p25*				1,680×1,680	39.65	20.99	36.38	_26.18_	30.80
Ours (LLaVA-Next)		CLIP-L14		Dynamic	**41.89**	21.85	**38.24**	**26.67**	**32.16**

Table 2. Leaderboard and performance comparison on LRS-VQA and MME-RealWorld-RS. "MME-RW-RS" indicates the MME-RealWorld-RS. "Data" refers to the total instruction data used during PT and SFT. "pX" indicates the max number is X for the pre-defined grids. "*method**" indicates we reproduce the SFT stage of existing methods using the 484k instruction data.

Setting	Color	Count	Position	Acc	FPS
anyres-p25	41.56	31.05	46.14	39.65	0.188
w/ PruMerge++	43.27	28.38	32.78	34.86	0.152
w/ VisionZip	42.71	24.55	34.55	33.98	0.183
w/ FastV	39.52	30.10	43.99	37.93	_0.192_
w/ PDrop	41.00	30.54	47.77	39.85	0.184
w/ prune (Ours)	43.98	30.42	49.16	_41.28_	0.165
DIP-3layer *w/ prune (Ours)*	44.08	30.94	49.26	**41.31**	**0.267**

Table 3. Comparison with different token reduction methods based on LLaVA-Next-Qwen2. To enable a fair comparison, we adopt the "anyres-p25" setting, where the maximum number of pre-defined grids is 25 (1,680×1,680 pixels). FPS is computed based on the inference time for 800 images from MME-Realworld-RS.

Setting	Vis. Tokens (Total)	Vis. Tokens (to LLM)	TFLOPs (B)
anyres-p144	83520	21312	243.37
w/ PruMerge++	83520	_5328_	_43.75_
w/ VisionZip	83520	9280	83.56
w/ FastV	83520	21312	109.21
w/ PDrop	83520	21312	101.62
w/ prune (Ours)	83520	5760	82.56
DIP-4layer *w/ prune (Ours)*	**55296**	**2376**	**36.61**

Table 4. Comparison of computational efficiency with different token reduction methods based on LLaVA-Next-Qwen2. We assume inferring a 4000×4000 pixel image (anyres-p144) and report the theoretical TFLOPs of vision tokens after the vision projector.

we reproduce other methods using the same 484k SFT data. Since the LLaVA-NeXT's training code is not open-source, we integrate the anyres strategy and Qwen2 into the LLaVA-1.5 framework, which serves as the codebase for our approach. All the experiments are conducted on 4 NVIDIA A100 80GB GPUs. For our method, the minimum length for DIP is 1,008 pixels. For Vicuna-1.5 and Qwen2, the N_{max} is set to 40 and 80, respectively. The vision token saving ratio α is 0.25, $\lambda_{hr}, \lambda_{mse}, \lambda_{kl}$ are 2.0, 1.0, 1.0,

respectively. The RFM-LLM layer pairs are $[1, 5, 11, 14]$ with distillation applied to the first and last pairs. More experimental details are in the Appendix A.2.2.

5.2. Leaderboard and Comparison

Leaderboard on LRS-VQA. We evaluate a total of 11 open-source LVLMs, including methods for high-resolution [27, 36, 76, 82], chain-of-thought reasoning [61], multiple visual encoders [30], and RS LVLMs [24, 37]. We also

Method	Drop Ratio	Color	Count	Pos	Acc
anyres-p25	0%	41.56	31.05	46.14	39.65
	25%	42.47	31.08	47.41	40.40
w/ prune (Ours)	50%	42.39	**31.24**	48.45	40.77
	75%	**43.98**	30.42	**49.16**	**41.28**
	90%	41.51	29.77	46.70	39.41

Table 5. Ablation study on different prune ratios with LLaVA-Next-Qwen2, when pruning vision tokens based on RFM results without DIP. This table demonstrates that pruning irrelevant tokens in high-resolution RSIs can improve performance.

Max Size	Color	Count	Pos	Acc	FPS
1,008×1,008	42.87	29.85	47.89	40.29	**0.271**
2,016×2,016	44.08	<u>30.94</u>	<u>49.26</u>	<u>41.31</u>	0.267
4,032×4,032	**44.86**	29.85	47.18	40.72	0.221
8,064×8,064	43.98	30.42	45.11	39.91	0.204
Dynamic	<u>44.70</u>	**31.00**	**49.72**	**41.89**	<u>0.238</u>

Table 6. Ablation study on fixing the number of DIP layers reached in inference with LLaVA-Next-Qwen2. Rows 1-4 correspond to fixing the number of DIP layers being 2-5, respectively.

RFM Layers	LLM Layers	Color	Count	Pos	Acc
3	[1,8,14]	41.35	28.30	47.89	39.27
4	[1,5,11,14]	**44.70**	**31.00**	**49.72**	**41.89**
5	[1,5,10,12,14]	43.98	29.36	48.13	40.58
6	[1,3,6,9,12,14]	42.31	31.08	47.18	40.26

Table 7. Ablation study on different RFM-LLM layer-pair configurations in MME-RealWorld-RS, with LLaVA-Next-Qwen2.

evaluate 3 closed-source MLLMs. Results in Tab. 2 indicate that LRS-VQA is more challenging than MME-RealWorld-RS on average, reflecting the complexities of large RSIs.

Comparison with high-resolution methods. As shown in Tab. 2, we select 5 different high resolution strategies, performing SFT on the same dataset for comparison. Our method performs better across all 4 datasets.

Comparison with token reduction methods. As shown in Tab. 3 and Tab. 4, we reproduce 4 plug-and-play methods for comparison on MME-RealWorld-RS. For Prune-Merge++ [50] and our RFM-based pruning, the retain ratio is 25%. For VisionZip [69], the number of retained tokens is 64. For PDrop [64] under Qwen2, pruning layers are set to [7,14,21]. Additionally, we employ 3-layer DIP, supporting up to 2,016×2,016 pixels, which improves accuracy by 1.46% and boosts FPS by 39% compared to other methods. For Tab. 4, we consistently use a 4-layer DIP. Since our method dynamically selects image tiles, we calculate the average number of tiles selected from similar size images in the dataset. Above results indicate that existing methods often overlook the high cost of processing many
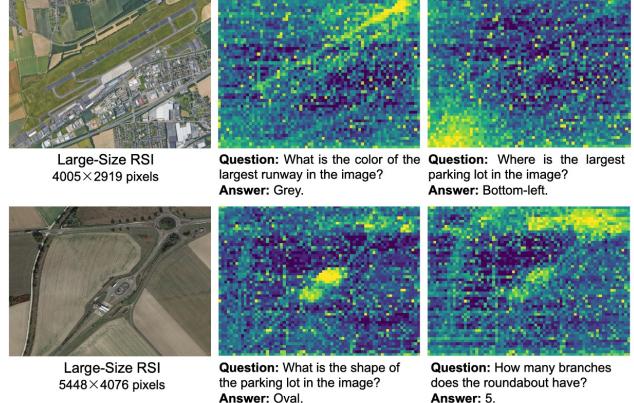

Figure 6. Text-related visual attention localization in the last layer if trained RFM under LLaVA-Next-Qwen2.

text-irrelevant image tiles in large images.

5.3. Ablation Results

We conducted ablation studies on the MME-RealWorld-RS, from the following aspects to perform an in-depth analysis:

Different ratios for RFM-based pruning. As shown in Tab. 5, a key finding is that in large RSIs, the complex background and the small foreground regions enable high pruning rates to deliver performance benefits.

Fixed DIP layers for inference. As shown in Tab. 6, we fix the number of DIP layers reached during inference. If an image's DIP is shallower than the specified number, the last layer is used. Results show that forcing traversal to higher resolutions can degrade performance since not all questions require image details. Therefore, our strategy dynamically selects the termination DIP layer based on the input text, balancing accuracy and efficiency.

Distillation settings for the RFM module. We explore the impact of different RFM-LLM layer-pairs in Tab. 7. Results show that introducing too many layers may hinder effective distillation and increase training and inference time, while too few layers may prevent RFM from effectively learning text-aware localization ability.

Visualization results. In Fig. 6, we visualize the attention maps generated by the trained RFM for vision tokens from initial input image tiles. The results demonstrate that text references to targets effectively guide the RFM's attention output, supporting our coarse-to-fine inference.

6. Conclusion

This paper presents a text-guided token pruning method tailored for efficiently processing large remote sensing images (RSIs). To address the limitations of existing high-resolution approaches when handling large RSIs, our method integrates the Region Focus Module (RFM) and Dynamic Image Pyramid (DIP) to focus on text-relevant key vision tokens while reducing computational overhead. Furthermore, we introduce a new benchmark, LRS-VQA,

with 7,333 QA pairs covering 8 question types, and features larger image sizes and a diverse range of question types.

Future work. Vision-language understanding of large RSIs remains challenging. Exploring alternative perspectives, such as long-context transfer from LLMs to LVLMs, to seek solutions is also meaningful.

References

[1] Josh Achiam, Steven Adler, Sandhini Agarwal, Lama Ahmad, Ilge Akkaya, Florencia Leoni Aleman, Diogo Almeida, Janko Altenschmidt, Sam Altman, Shyamal Anadkat, et al. Gpt-4 technical report. *arXiv preprint arXiv:2303.08774*, 2023. 1

[2] Open AI. Hello gpt-4o. 2024. 7

[3] AI Anthropic. Claude 3.5 sonnet model card addendum. page 3, 2024. 7

[4] Kazi Hasan Ibn Arif, JinYi Yoon, Dimitrios S. Nikolopoulos, Hans Vandierendonck, Deepu John, and Bo Ji. Hired: Attention-guided token dropping for efficient inference of high-resolution vision-language models, 2024. 2

[5] Jinze Bai, Shuai Bai, Shusheng Yang, Shijie Wang, Sinan Tan, Peng Wang, Junyang Lin, Chang Zhou, and Jingren Zhou. Qwen-vl: A frontier large vision-language model with versatile abilities. *arXiv preprint arXiv:2308.12966*, 2023. 2

[6] Liang Chen, Haozhe Zhao, Tianyu Liu, Shuai Bai, Junyang Lin, Chang Zhou, and Baobao Chang. An image is worth 1/2 tokens after layer 2: Plug-and-play inference acceleration for large vision-language models. In *European Conference on Computer Vision*, pages 19–35. Springer, 2024. 2

[7] Zhe Chen, Weiyun Wang, Yue Cao, Yangzhou Liu, Zhangwei Gao, Erfei Cui, Jinguo Zhu, Shenglong Ye, Hao Tian, Zhaoyang Liu, et al. Expanding performance boundaries of open-source multimodal models with model, data, and test-time scaling. *arXiv preprint arXiv:2412.05271*, 2024. 1

[8] Zhe Chen, Weiyun Wang, Hao Tian, Shenglong Ye, Zhangwei Gao, Erfei Cui, Wenwen Tong, Kongzhi Hu, Jiapeng Luo, Zheng Ma, et al. How far are we to gpt-4v? closing the gap to commercial multimodal models with open-source suites. *Science China Information Sciences*, 67(12):220101, 2024. 2, 3

[9] Wei-Lin Chiang, Zhuohan Li, Zi Lin, Ying Sheng, Zhanghao Wu, Hao Zhang, Lianmin Zheng, Siyuan Zhuang, Yonghao Zhuang, Joseph E. Gonzalez, Ion Stoica, and Eric P. Xing. Vicuna: An open-source chatbot impressing gpt-4 with 90%* chatgpt quality, 2023. 1

[10] Muhammad Sohail Danish, Muhammad Akhtar Munir, Syed Roshaan Ali Shah, Kartik Kuckreja, Fahad Shahbaz Khan, Paolo Fraccaro, Alexandre Lacoste, and Salman Khan. Geobench-vlm: Benchmarking vision-language models for geospatial tasks. *arXiv preprint arXiv:2411.19325*, 2024. 1

[11] Tri Dao, Dan Fu, Stefano Ermon, Atri Rudra, and Christopher Ré. Flashattention: Fast and memory-efficient exact attention with io-awareness. *Advances in neural information processing systems*, 35:16344–16359, 2022. 5

[12] DeepSeek-AI, Daya Guo, Dejian Yang, Haowei Zhang, Junxiao Song, Ruoyu Zhang, Runxin Xu, Qihao Zhu, et al.

[13] Jian Ding, Nan Xue, Gui-Song Xia, Xiang Bai, Wen Yang, Michael Ying Yang, Serge Belongie, Jiebo Luo, Mihai Datcu, Marcello Pelillo, et al. Object detection in aerial images: A large-scale benchmark and challenges. *IEEE transactions on pattern analysis and machine intelligence*, 44(11): 7778–7796, 2021. 6

[14] Peiyan Dong, Mengshu Sun, Alec Lu, Yanyue Xie, Kenneth Liu, Zhenglun Kong, Xin Meng, Zhengang Li, Xue Lin, Zhenman Fang, et al. Heatvit: Hardware-efficient adaptive token pruning for vision transformers. In *2023 IEEE International Symposium on High-Performance Computer Architecture (HPCA)*, pages 442–455. IEEE, 2023. 2

[15] Abhimanyu Dubey, Abhinav Jauhri, Abhinav Pandey, Abhishek Kadian, Ahmad Al-Dahle, Aiesha Letman, Akhil Mathur, Alan Schelten, Amy Yang, Angela Fan, et al. The llama 3 herd of models. *arXiv preprint arXiv:2407.21783*, 2024. 1

[16] Zonghao Guo, Ruyi Xu, Yuan Yao, Junbo Cui, Zanlin Ni, Chunjiang Ge, Tat-Seng Chua, Zhiyuan Liu, and Gao Huang. Llava-uhd: an lmm perceiving any aspect ratio and high-resolution images. In *European Conference on Computer Vision*, pages 390–406. Springer, 2025. 2, 3

[17] Yuhang Han, Xuyang Liu, Pengxiang Ding, Donglin Wang, Honggang Chen, Qingsen Yan, and Siteng Huang. Rethinking token reduction in mllms: Towards a unified paradigm for training-free acceleration. *arXiv preprint arXiv:2411.17686*, 2024. 2

[18] Runhui Huang, Xinpeng Ding, Chunwei Wang, Jianhua Han, Yulong Liu, Hengshuang Zhao, Hang Xu, Lu Hou, Wei Zhang, and Xiaodan Liang. Hires-llava: Restoring fragmentation input in high-resolution large vision-language models. *arXiv preprint arXiv:2407.08706*, 2024. 2

[19] Drew A Hudson and Christopher D Manning. Gqa: A new dataset for real-world visual reasoning and compositional question answering. In *Proceedings of the IEEE/CVF conference on Computer Vision and Pattern Recognition*, pages 6700–6709, 2019. 6

[20] Omri Kaduri, Shai Bagon, and Tali Dekel. What's in the image? a deep-dive into the vision of vision language models. *arXiv preprint arXiv:2411.17491*, 2024. 3, 4

[21] Sehoon Kim, Sheng Shen, David Thorsley, Amir Gholami, Woosuk Kwon, Joseph Hassoun, and Kurt Keutzer. Learned token pruning for transformers. In *Proceedings of the 28th ACM SIGKDD Conference on Knowledge Discovery and Data Mining*, pages 784–794, 2022. 2

[22] Alexander Kirillov, Eric Mintun, Nikhila Ravi, Hanzi Mao, Chloe Rolland, Laura Gustafson, Tete Xiao, Spencer Whitehead, Alexander C Berg, Wan-Yen Lo, et al. Segment anything. In *Proceedings of the IEEE/CVF international conference on computer vision*, pages 4015–4026, 2023. 2

[23] Zhenglun Kong, Peiyan Dong, Xiaolong Ma, Xin Meng, Wei Niu, Mengshu Sun, Xuan Shen, Geng Yuan, Bin Ren, Hao Tang, et al. Spvit: Enabling faster vision transformers via latency-aware soft token pruning. In *European conference on computer vision*, pages 620–640. Springer, 2022. 2

Deepseek-r1: Incentivizing reasoning capability in llms via reinforcement learning, 2025. 1

[24] Kartik Kuckreja, Muhammad Sohail Danish, Muzammal Naseer, Abhijit Das, Salman Khan, and Fahad Shahbaz Khan. Geochat: Grounded large vision-language model for remote sensing. *Proceedings of the IEEE Conference on Computer Vision and Pattern Recognition*, 2024. 2, 7

[25] Bo Li, Yuanhan Zhang, Dong Guo, Renrui Zhang, Feng Li, Hao Zhang, Kaichen Zhang, Peiyuan Zhang, Yanwei Li, Ziwei Liu, et al. Llava-onevision: Easy visual task transfer. *arXiv preprint arXiv:2408.03326*, 2024. 1, 2, 7

[26] Junnan Li, Dongxu Li, Silvio Savarese, and Steven Hoi. Blip-2: Bootstrapping language-image pre-training with frozen image encoders and large language models. In *International conference on machine learning*, pages 19730–19742. PMLR, 2023. 2

[27] Junyan Li, Delin Chen, Tianle Cai, Peihao Chen, Yining Hong, Zhenfang Chen, Yikang Shen, and Chuang Gan. Flex-attention for efficient high-resolution vision-language models. In *European Conference on Computer Vision*, pages 286–302. Springer, 2024. 2, 7

[28] Qingyun Li, Yushi Chen, Xinya Shu, Dong Chen, Xin He, Yu Yi, and Xue Yang. A simple aerial detection baseline of multimodal language models. *arXiv preprint arXiv:2501.09720*, 2025. 1

[29] Wentong Li, Yuqian Yuan, Jian Liu, Dongqi Tang, Song Wang, Jie Qin, Jianke Zhu, and Lei Zhang. Tokenpacker: Efficient visual projector for multimodal llm. *arXiv preprint arXiv:2407.02392*, 2024. 2

[30] Yanwei Li, Yuechen Zhang, Chengyao Wang, Zhisheng Zhong, Yixin Chen, Ruihang Chu, Shaoteng Liu, and Jiaya Jia. Mini-gemini: Mining the potential of multi-modality vision language models. *arXiv:2403.18814*, 2023. 2, 7

[31] Yansheng Li, Junwei Luo, Yongjun Zhang, Yihua Tan, Jin-Gang Yu, and Song Bai. Learning to holistically detect bridges from large-size vhr remote sensing imagery. *IEEE Transactions on Pattern Analysis and Machine Intelligence*, 2024. 2, 5, 6

[32] Yanwei Li, Chengyao Wang, and Jiaya Jia. Llama-vid: An image is worth 2 tokens in large language models. 2024. 2

[33] Yansheng Li, Linlin Wang, Tingzhu Wang, Xue Yang, Junwei Luo, Qi Wang, Youming Deng, Wenbin Wang, Xian Sun, Haifeng Li, Bo Dang, Yongjun Zhang, Yi Yu, and Yan Junchi. Star: A first-ever dataset and a large-scale benchmark for scene graph generation in large-size satellite imagery. *IEEE Transactions on Pattern Analysis and Machine Intelligence*, 2024. 2, 5, 6

[34] Zhang Li, Biao Yang, Qiang Liu, Zhiyin Ma, Shuo Zhang, Jingxu Yang, Yabo Sun, Yuliang Liu, and Xiang Bai. Monkey: Image resolution and text label are important things for large multi-modal models. In *Proceedings of the IEEE/CVF Conference on Computer Vision and Pattern Recognition*, pages 26763–26773, 2024. 2

[35] Haotian Liu, Chunyuan Li, Yuheng Li, and Yong Jae Lee. Improved baselines with visual instruction tuning. *arXiv preprint arXiv:2310.03744*, 2023. 1, 2, 7

[36] Haotian Liu, Chunyuan Li, Qingyang Wu, and Yong Jae Lee. Visual instruction tuning. *Advances in Neural Information Processing Systems*, 36, 2024. 6, 7

[37] Xu Liu and Zhouhui Lian. Rsunivlm: A unified vision language model for remote sensing via granularity-oriented mixture of experts. *arXiv preprint arXiv:2412.05679*, 2024. 7

[38] Yuliang Liu, Biao Yang, Qiang Liu, Zhang Li, Zhiyin Ma, Shuo Zhang, and Xiang Bai. Textmonkey: An ocr-free large multimodal model for understanding document. *arXiv preprint arXiv:2403.04473*, 2024. 2

[39] Zhuang Liu, Hanzi Mao, Chao-Yuan Wu, Christoph Feichtenhofer, Trevor Darrell, and Saining Xie. A convnet for the 2020s. *Proceedings of the IEEE/CVF Conference on Computer Vision and Pattern Recognition (CVPR)*, 2022. 2

[40] Sylvain Lobry, Diego Marcos, Jesse Murray, and Devis Tuia. Rsvqa: Visual question answering for remote sensing data. *IEEE Transactions on Geoscience and Remote Sensing*, 58 (12):8555–8566, 2020. 6

[41] Gen Luo, Xue Yang, Wenhan Dou, Zhaokai Wang, Jiawen Liu, Jifeng Dai, Yu Qiao, and Xizhou Zhu. Mono-internvl: Pushing the boundaries of monolithic multimodal large language models with endogenous visual pre-training. *arXiv preprint arXiv:2410.08202*, 2024. 3

[42] Gen Luo, Yiyi Zhou, Yuxin Zhang, Xiawu Zheng, Xiaoshuai Sun, and Rongrong Ji. Feast your eyes: Mixture-of-resolution adaptation for multimodal large language models. *arXiv preprint arXiv:2403.03003*, 2024. 2

[43] Junwei Luo, Zhen Pang, Yongjun Zhang, Tingzhu Wang, Linlin Wang, Bo Dang, Jiangwei Lao, Jian Wang, Jingdong Chen, Yihua Tan, et al. Skysensegpt: A fine-grained instruction tuning dataset and model for remote sensing vision-language understanding. *arXiv preprint arXiv:2406.10100*, 2024. 1

[44] Lingchen Meng, Hengduo Li, Bor-Chun Chen, Shiyi Lan, Zuxuan Wu, Yu-Gang Jiang, and Ser-Nam Lim. Adavit: Adaptive vision transformers for efficient image recognition. In *Proceedings of the IEEE/CVF conference on computer vision and pattern recognition*, pages 12309–12318, 2022. 2

[45] George A Miller. Wordnet: a lexical database for english. *Communications of the ACM*, 38(11):39–41, 1995. 6

[46] Dilxat Muhtar, Zhenshi Li, Feng Gu, Xueliang Zhang, and Pengfeng Xiao. Lhrs-bot: Empowering remote sensing with vgi-enhanced large multimodal language model. In *European Conference on Computer Vision*, pages 440–457. Springer, 2024. 1

[47] OpenAI. Gpt-4v(ision) system card. 2023. 6

[48] Yongming Rao, Wenliang Zhao, Benlin Liu, Jiwen Lu, Jie Zhou, and Cho-Jui Hsieh. Dynamicvit: Efficient vision transformers with dynamic token sparsification. *Advances in neural information processing systems*, 34:13937–13949, 2021. 2

[49] Akashah Shabbir, Mohammed Zumri, Mohammed Bennamoun, Fahad S Khan, and Salman Khan. Geopixel: Pixel grounding large multimodal model in remote sensing. *arXiv preprint arXiv:2501.13925*, 2025. 2

[50] Yuzhang Shang, Mu Cai, Bingxin Xu, Yong Jae Lee, and Yan Yan. Llava-prumerge: Adaptive token reduction for efficient large multimodal models. *arXiv preprint arXiv:2403.15388*, 2024. 2, 8

10

[51] Hao Shao, Shengju Qian, Han Xiao, Guanglu Song, Zhuofan Zong, Letian Wang, Yu Liu, and Hongsheng Li. Visual cot: Advancing multi-modal language models with a comprehensive dataset and benchmark for chain-of-thought reasoning. *Advances in Neural Information Processing Systems*, 37:8612–8642, 2025. 2

[52] Haozhan Shen, Kangjia Zhao, Tiancheng Zhao, Ruochen Xu, Zilun Zhang, Mingwei Zhu, and Jianwei Yin. Zoomeye: Enhancing multimodal llms with human-like zooming capabilities through tree-based image exploration. *arXiv preprint arXiv:2411.16044*, 2024. 2

[53] Sagar Soni, Akshay Dudhane, Hiyam Debary, Mustansar Fiaz, Muhammad Akhtar Munir, Muhammad Sohail Danish, Paolo Fraccaro, Campbell D Watson, Levente J Klein, Fahad Shahbaz Khan, et al. Earthdial: Turning multi-sensory earth observations to interactive dialogues. *arXiv preprint arXiv:2412.15190*, 2024. 2

[54] Xian Sun, Peijin Wang, Zhiyuan Yan, Feng Xu, Ruiping Wang, Wenhui Diao, Jin Chen, Jihao Li, Yingchao Feng, Tao Xu, et al. Fair1m: A benchmark dataset for fine-grained object recognition in high-resolution remote sensing imagery. *ISPRS Journal of Photogrammetry and Remote Sensing*, 184:116–130, 2022. 5

[55] Peter Tong, Ellis Brown, Penghao Wu, Sanghyun Woo, Adithya Jairam Vedagiri IYER, Sai Charitha Akula, Shusheng Yang, Jihan Yang, Manoj Middepogu, Ziteng Wang, et al. Cambrian-1: A fully open, vision-centric exploration of multimodal llms. *Advances in Neural Information Processing Systems*, 37:87310–87356, 2025. 2

[56] Junjue Wang, Zhuo Zheng, Zihang Chen, Ailong Ma, and Yanfei Zhong. Earthvqa: Towards queryable earth via relational reasoning-based remote sensing visual question answering. In *Proceedings of the AAAI Conference on Artificial Intelligence*, pages 5481–5489, 2024. 2

[57] Peng Wang, Shuai Bai, Sinan Tan, Shijie Wang, Zhihao Fan, Jinze Bai, Keqin Chen, Xuejing Liu, Jialin Wang, Wenbin Ge, et al. Qwen2-vl: Enhancing vision-language model's perception of the world at any resolution. *arXiv preprint arXiv:2409.12191*, 2024. 1, 6, 7

[58] Wenbin Wang, Liang Ding, Minyan Zeng, Xiabin Zhou, Li Shen, Yong Luo, and Dacheng Tao. Divide, conquer and combine: A training-free framework for high-resolution image perception in multimodal large language models. *arXiv preprint*, 2024. 2

[59] Xidong Wang, Dingjie Song, Shunian Chen, Chen Zhang, and Benyou Wang. Longllava: Scaling multi-modal llms to 1000 images efficiently via a hybrid architecture. *arXiv preprint arXiv:2409.02889*, 2024. 2

[60] Siyuan Wei, Tianzhu Ye, Shen Zhang, Yao Tang, and Jiajun Liang. Joint token pruning and squeezing towards more aggressive compression of vision transformers. In *Proceedings of the IEEE/CVF conference on computer vision and pattern recognition*, pages 2092–2101, 2023. 2

[61] Penghao Wu and Saining Xie. V*: Guided visual search as a core mechanism in multimodal llms. In *Proceedings of the IEEE/CVF Conference on Computer Vision and Pattern Recognition*, pages 13084–13094, 2024. 2, 7

[62] Aoran Xiao, Weihao Xuan, Junjue Wang, Jiaxing Huang, Dacheng Tao, Shijian Lu, and Naoto Yokoya. Foundation models for remote sensing and earth observation: A survey. *arXiv preprint arXiv:2410.16602*, 2024. 2

[63] Junbin Xiao, Xindi Shang, Angela Yao, and Tat-Seng Chua. Next-qa: Next phase of question-answering to explaining temporal actions. In *Proceedings of the IEEE/CVF conference on computer vision and pattern recognition*, pages 9777–9786, 2021. 6

[64] Long Xing, Qidong Huang, Xiaoyi Dong, Jiajie Lu, Pan Zhang, Yuhang Zang, Yuhang Cao, Conghui He, Jiaqi Wang, Feng Wu, et al. Pyramiddrop: Accelerating your large vision-language models via pyramid visual redundancy reduction. *arXiv preprint arXiv:2410.17247*, 2024. 2, 4, 8

[65] Xizhe Xue, Guoting Wei, Hao Chen, Haokui Zhang, Feng Lin, Chunhua Shen, and Xiao Xiang Zhu. Reo-vlm: Transforming vlm to meet regression challenges in earth observation. *arXiv preprint arXiv:2412.16583*, 2024. 1

[66] Dawei Yan, Pengcheng Li, Yang Li, Hao Chen, Qingguo Chen, Weihua Luo, Wei Dong, Qingsen Yan, Haokui Zhang, and Chunhua Shen. Tg-llava: Text guided llava via learnable latent embeddings. *arXiv preprint arXiv:2409.09564*, 2024. 2

[67] An Yang, Baosong Yang, Beichen Zhang, Binyuan Hui, Bo Zheng, Bowen Yu, Chengyuan Li, Dayiheng Liu, Fei Huang, Haoran Wei, Huan Lin, Jian Yang, Jianhong Tu, Jianwei Zhang, Jianxin Yang, Jiaxi Yang, Jingren Zhou, Junyang Lin, Kai Dang, Keming Lu, Keqin Bao, Kexin Yang, Le Yu, Mei Li, Mingfeng Xue, Pei Zhang, Qin Zhu, Rui Men, Runji Lin, Tianhao Li, Tingyu Xia, Xingzhang Ren, Xuancheng Ren, Yang Fan, Yang Su, Yichang Zhang, Yu Wan, Yuqiong Liu, Zeyu Cui, Zhenru Zhang, and Zihan Qiu. Qwen2.5 technical report. *arXiv preprint arXiv:2412.15115*, 2024. 1

[68] Jianwei Yang, Hao Zhang, Feng Li, Xueyan Zou, Chunyuan Li, and Jianfeng Gao. Set-of-mark prompting unleashes extraordinary visual grounding in gpt-4v, 2023. 6

[69] Senqiao Yang, Yukang Chen, Zhuotao Tian, Chengyao Wang, Jingyao Li, Bei Yu, and Jiaya Jia. Visionzip: Longer is better but not necessary in vision language models. *arXiv preprint arXiv:2412.04467*, 2024. 2, 8

[70] Linli Yao, Lei Li, Shuhuai Ren, Lean Wang, Yuanxin Liu, Xu Sun, and Lu Hou. Deco: Decoupling token compression from semantic abstraction in multimodal large language models. *arXiv preprint arXiv:2405.20985*, 2024. 2

[71] Deming Ye, Yankai Lin, Yufei Huang, and Maosong Sun. Tr-bert: Dynamic token reduction for accelerating bert inference. *arXiv preprint arXiv:2105.11618*, 2021. 2

[72] Jiabo Ye, Anwen Hu, Haiyang Xu, Qinghao Ye, Ming Yan, Guohai Xu, Chenliang Li, Junfeng Tian, Qi Qian, Ji Zhang, et al. Ureader: Universal ocr-free visually-situated language understanding with multimodal large language model. In *The 2023 Conference on Empirical Methods in Natural Language Processing*, 2023. 2

[73] Weihao Ye, Qiong Wu, Wenhao Lin, and Yiyi Zhou. Fit and prune: Fast and training-free visual token pruning for multi-modal large language models. *arXiv preprint arXiv:2409.10197*, 2024. 2, 3, 4

[74] Xubing Ye, Yukang Gan, Xiaoke Huang, Yixiao Ge, Ying Shan, and Yansong Tang. Voco-llama: Towards vision compression with large language models. *arXiv preprint arXiv:2406.12275*, 2024. 2

[75] Yang Zhan, Zhitong Xiong, and Yuan Yuan. Skyeyegpt: Unifying remote sensing vision-language tasks via instruction tuning with large language model. *ISPRS Journal of Photogrammetry and Remote Sensing*, 221:64–77, 2025. 1

[76] Pan Zhang, Xiaoyi Dong, Yuhang Zang, Yuhang Cao, Rui Qian, Lin Chen, Qipeng Guo, Haodong Duan, Bin Wang, Linke Ouyang, Songyang Zhang, Wenwei Zhang, Yining Li, Yang Gao, Peng Sun, Xinyue Zhang, Wei Li, Jingwen Li, Wenhai Wang, Hang Yan, Conghui He, Xingcheng Zhang, Kai Chen, Jifeng Dai, Yu Qiao, Dahua Lin, and Jiaqi Wang. Internlm-xcomposer-2.5: A versatile large vision language model supporting long-contextual input and output. *arXiv preprint arXiv:2407.03320*, 2024. 2, 7

[77] Shaolei Zhang, Qingkai Fang, Zhe Yang, and Yang Feng. Llava-mini: Efficient image and video large multimodal models with one vision token. *arXiv preprint arXiv:2501.03895*, 2025. 2

[78] Wei Zhang, Miaoxin Cai, Tong Zhang, Yin Zhuang, Jun Li, and Xuerui Mao. Earthmarker: A visual prompting multimodal large language model for remote sensing. *IEEE Transactions on Geoscience and Remote Sensing*, 2024. 2

[79] Wei Zhang, Miaoxin Cai, Tong Zhang, Yin Zhuang, and Xuerui Mao. Earthgpt: A universal multi-modal large language model for multi-sensor image comprehension in remote sensing domain. *arXiv preprint arXiv:2401.16822*, 2024. 1

[80] Yuan Zhang, Chun-Kai Fan, Junpeng Ma, Wenzhao Zheng, Tao Huang, Kuan Cheng, Denis Gudovskiy, Tomoyuki Okuno, Yohei Nakata, Kurt Keutzer, et al. Sparsevlm: Visual token sparsification for efficient vision-language model inference. *arXiv preprint arXiv:2410.04417*, 2024. 2, 5

[81] Yipeng Zhang, Yifan Liu, Zonghao Guo, Yidan Zhang, Xuesong Yang, Chi Chen, Jun Song, Bo Zheng, Yuan Yao, Zhiyuan Liu, et al. Llava-uhd v2: an mllm integrating high-resolution feature pyramid via hierarchical window transformer. *arXiv preprint arXiv:2412.13871*, 2024. 7

[82] Yi-Fan Zhang, Qingsong Wen, Chaoyou Fu, Xue Wang, Zhang Zhang, Liang Wang, and Rong Jin. Beyond llava-hd: Diving into high-resolution large multimodal models. *arXiv preprint arXiv:2406.08487*, 2024. 2, 7

[83] Yi-Fan Zhang, Huanyu Zhang, Haochen Tian, Chaoyou Fu, Shuangqing Zhang, Junfei Wu, Feng Li, Kun Wang, Qingsong Wen, Zhang Zhang, et al. Mme-realworld: Could your multimodal llm challenge high-resolution real-world scenarios that are difficult for humans? *arXiv preprint arXiv:2408.13257*, 2024. 2, 6

[84] Zilun Zhang, Haozhan Shen, Tiancheng Zhao, Yuhao Wang, Bin Chen, Yuxiang Cai, Yongheng Shang, and Jianwei Yin. Enhancing ultra high resolution remote sensing imagery analysis with imagerag. *arXiv preprint arXiv:2411.07688*, 2024. 2

[85] Yue Zhou, Litong Feng, Yiping Ke, Xue Jiang, Junchi Yan, Xue Yang, and Wayne Zhang. Towards vision-language geo-foundation models: A survey. *arXiv preprint arXiv:2406.09385*, 2024. 2